Th. Wegner, B. Geiger, R. Foest, et al.

View Online    Export Citation    CrossMark

## ARTICLES YOU MAY BE INTERESTED IN
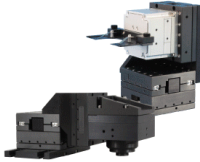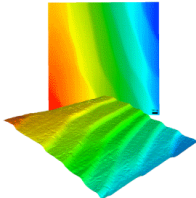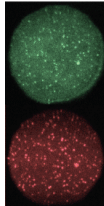
Nanopositioning Systems

Modular Motion Control

AFM and NSOM Instruments

Single Molecule Microscopes

MCL MAD CITY LABS INC.
www.madcitylabs.com

# Preparation, analysis, and application of coated glass targets for the Wendelstein 7-X laser blow-off system

View Online    Export Citation    CrossMark

Th. Wegner,[1,a] B. Geiger,[1,b] R. Foest,[2] A. Jansen van Vuuren,[3] V. R. Winters,[1,4] C. Biedermann,[1] R. Burhenn,[1] B. Buttenschön,[1] G. Cseh,[5] I. Joda,[4] G. Kocsis,[5] F. Kunkel,[1] A. Quade,[2] J. Schäfer,[2] O. Schmitz,[4] T. Szepesi,[5] and W7-X Team[1,c]

### AFFILIATIONS

[1] Max-Planck Institute for Plasma Physics, 17491 Greifswald, Germany
[2] Leibniz Institut für Plasmaforschung und Technologie e.V., 17489 Greifswald, Germany
[3] Max-Planck Institute for Plasma Physics, 85748 Garching, Germany
[4] University of Wisconsin-Madison, Madison, Wisconsin 53706, USA
[5] Wigner Research Center for Physics, 1121 Budapest, Hungary

[a] Author to whom correspondence should be addressed: thomas.wegner@ipp.mpg.de and physics@thwegner.com
[b] Present address: University of Wisconsin-Madison, WI 53706, USA.
[c] Author list in T. Klinger *et al.*, Nucl. Fusion **59**, 112004 (2019).

### ABSTRACT

Coated glass targets are a key component of the Wendelstein 7-X laser blow-off system that is used for impurity transport studies. The preparation and analysis of these glass targets as well as their performance is examined in this paper. The glass targets have a high laser damage threshold and are coated via physical vapor deposition with $\mu$m thick films. In addition, nm-thin layers of Ti are used as an interface layer for improved ablation efficiency and reduced coating stress. Hence, the metallic or ceramic coating has a lateral homogeneity within 2% and contaminants less than 5%, being optimal for laser ablation processing. With this method, a short (few ms) and well defined pulse of impurities with about $10^{17}$ particles can be injected close to the last closed flux surface of Wendelstein 7-X. In particular, a significant amount of atoms with a velocity of about 1 km/s enters the plasma within 1 ms. The atoms are followed by a negligible concentration of slower clusters and macro-particles. This qualifies the use of the targets and applied laser settings for impurity transport studies with the laser blow-off system in Wendelstein 7-X.

## I. INTRODUCTION

The removal of thin absorbing layers, e.g., metals, from transparent substrates such as glasses by means of laser irradiation impact is called "laser ablation" or "laser blow-off" (LBO). This method can be divided into different cases depending on the side of irradiation, thicknesses of the layers and substrates, and laser properties such as the pulse duration and wavelength.[1] These different ablation processes enable a wide-spread field of applications. In particular, the laser blow-off technique has been applied in fusion experiments for impurity transport studies,[2–7] for electron heat transport investigation,[8,9] and for plasma temperature and density measurements at the plasma edge.[10–13] It has also been used for studying atomic processes,[14–18] patterning of thin film solar cells,[19,20] and laser induced metal deposition.[21]

The LBO system in the stellarator Wendelstein 7-X (W7-X)[22] is applied to inject non-intrinsic and non-recycling impurities to study their transport through the plasma.[23–25] The understanding of impurity transport is of utmost importance since impurities may lead, under specific conditions, to a degradation of the overall plasma performance or early pulse termination by increased radiative losses and dilution effects.[26,27] The experimental setup of the W7-X LBO

system, as previously described by Wegner et al.,[7] consists of a high energy laser, optical components, and a glass target holder that is mounted on a manipulator to move the targets into the plasma vessel 600 mm away from the last closed flux surface (LCFS) being the boundary of the confined plasma region. The laser beam (Nd:YAG laser at 1064 nm with a pulse energy of 1 J and a pulse duration of 6 ns) is guided through movable lenses and mirrors to the glass targets. The glass targets are mounted with the coating facing toward the plasma side. The laser beam goes through the glass, hits the coating from behind, and generates a small plasma on the glass surface.[1] This small plasma expands, blows-off, and accelerates the ablated material, independently of the laser beam incident angle, perpendicular to the glass surface toward the plasma. Hence, the here considered LBO process can be classified as thin film glass side ablation. The application of LBO for impurity transport studies is advantageous since this method allows for a repetitive and controlled injection of a well known amount of trace impurities with a defined spatial and temporal source function. However, the proper choice of laser settings and target materials has a very strong impact on the success of LBO experiments and requires detailed understanding of micro-scale and macro-scale properties. The optimization of the ablation process is proceeded via iterative ablation tests combined with the analysis of the ablated spots on the glass targets.

Hence, this paper describes the preparation of targets and the optimization of laser settings for the use of a glass side LBO for impurity transport studies in W7-X. Section II focuses on the applied coating methods, while Sec. III presents experimental results regarding the coating thickness and composition. The usage of the prepared glass targets for LBO impurity injection in W7-X is characterized in Sec. IV of this paper. We can show that these targets are highly suitable for that specific purpose, which enables an important research field for fusion devices with the potential of steady state operation. Finally, a short summary is given.

## II. PREPARATION OF LBO TARGETS

The choice of appropriate glasses is a mandatory task for the high energy LBO of thin films. The different glass types can be classified according to their material, volume purity, surface quality, and polish degree. Additionally, different key attributes such as transmittance, homogeneity, inclusion, and laser damage threshold result from the above-mentioned classification. Hence, a suitable glass for a thin film glass side LBO has a high transmittance for the laser wavelength, a good homogeneity for a suitable and adherent coating, and low inclusions to guarantee a high laser damage threshold. Here, fused silica glass targets (Corning® HPFS® 7980-5f, $45 \times 45 \times 2 \text{ mm}^3$) are chosen for LBO application and are coated via physical vapor deposition (PVD).

Thin coatings suitable for laser ablation are commonly deposited using PVD methods where the film material is provided from a solid target. Typical techniques are the direct current magnetron sputtering (MS) and electron beam evaporation (EB). The target material is sputtered by impinging ions (MS) or evaporated by an electron beam directed to a crucible that contains the target material (EB). Under low pressure conditions, the evaporated material is transported toward the substrate, where it condenses on the surface forming a thin coating (e.g., of the ablation material as in this case)

with typical growth rates of a few nm/s.[29] The process conditions have a major impact on the morphology and mechanical and optical properties of the resulting thin film. In the case of MS, the parameter governing the film properties is the amount of applied momentum and energy provided by the ions that are formed in the plasma and accelerated toward the target surface. In particular, the reduction of the bias voltage from 100 V to 60 V is a crucial optimization step to achieve homogeneous coatings with adequate adhesion. Basically, the process condition for EB is chosen to ensure a uniform material evaporation while maintaining a desirable high deposition rate of up to 4 nm/s and a preferably low temperature of the crucible. Additionally, a controlled substrate temperature can contribute to the reduction of inner stress. The deposition process itself heats up the substrate to temperatures of up to 450 K. Hence, the substrate is pre-conditioned thermally to 450 K prior to deposition to avoid accumulation of thermal stress.

For some materials, see the brackets in Table I, a thin interface layer of Ti is additionally deposited on the glass prior to the actual coating used for ablation and injection. This slightly reduces the purity of the coating but improves the ablation performance since the applied laser radiation is absorbed significantly better on Ti than on Cu or Fe, for example. Hence, this interface layer enables the ablation of the material with the applied laser energy density (see Sec. III) with one shot. Without having a Ti interface layer for coating materials that have a high reflection coefficient for the used laser wavelength such as Cu or Fe, a complete ablation with one shot is not possible even if the laser energy density is doubled. Additionally, the film adhesion on the glass surface can be significantly enhanced with a Ti interface layer. Moreover, it is observed that the inner stress of the film can be alleviated by an intermediate layer that interrupts the columnar growth. Depending on the material and the coating thickness, this columnar growth can lead to an inhomogeneous coating with a broken surface. Hence, the deposition of a 5 $\mu$m thick film is suspended after the actual film has reached a thickness of 2.5 $\mu$m for the deposition of a 50 nm Ti interlayer. Afterward, the deposition of the actual film is continued until the full thickness of 5 $\mu$m is reached.

TABLE I. Overview of the coating and interface (in brackets) materials that were successfully applied to the W7-X LBO system together with the used PVD method (MS: magnetron sputtering and EB: electron beam evaporation) and the achieved coating thickness.

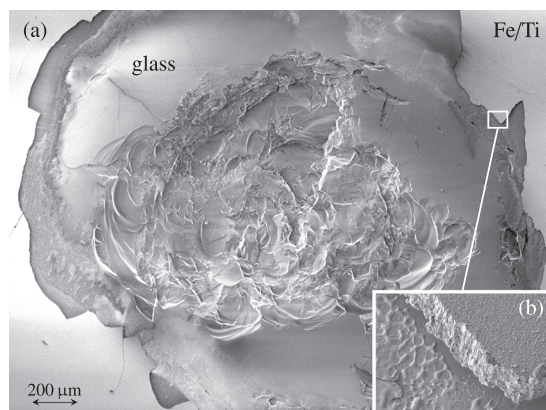| Material (interface) | PVD method | Thickness ($\mu$m) |
|---|---|---|
| $B_4C$ (Ti) | MS | 6.2 (0.05) |
| Cu (Ti) | EB | 2 (0.05) |
| Fe | MS | 2 |
| Fe (Ti)[a] | EB | 5 (0.1) |
| Mo | MS | 2 |
| Mo (Ti) | EB | 3.5 (0.05) |
| Ni | EB | 2 |
| Si | MS | 5 |
| Ti[a] | EB | 2 and 5 |
| W | MS | 2.1 |

[a]Coating materials are analyzed in detail in this paper.

To study the impurity transport and especially the impact of the nuclear charge,[28] different materials are deposited with the above-mentioned PVD methods on the glass targets. The materials listed in Table I were injected into the plasma vessel of W7-X during the operation phase OP1.2 owing to their well-studied emission characteristics. However, the following analysis and the characterization of the LBO injection focus only on Fe/Ti and Ti coated glass targets, without limiting the generality.

## III. ANALYSIS OF THE COATED GLASS TARGETS

The analysis of the glass target and the coating is important to verify the applicability for LBO injections in a fusion device. Especially, the laser damage threshold of glasses is a major property with respect to the application of high energy LBO. Hence, the glass targets that are used for the following experiments presented in this paper are analyzed with respect to their laser damage threshold. For this, the laser energy density on the target is varied to determine the threshold values by shooting once on the coated glass target from the glass side. Up to a laser energy density of 13 J/cm$^2$, the surface of the glass is not affected by the laser. A slight increase to 14 J/cm$^2$ leads to a well visible damage of the coating side surface only, see Fig. 1(a). At a laser energy of 90 J/cm$^2$, the glass target gets cracks and the surfaces on both sides of the glass are damaged. However, the typical applied laser energy density to W7-X of 8 J/cm$^2$ (4 mm spot diameter at 1 J laser pulse energy) is low enough not to damage the glass but high enough to fully ablate the coating. Exemplarily, a full ablation of an Fe/Ti (thickness of 5 $\mu$m/0.1 $\mu$m) coating is observed for laser energy densities higher than 4 J/cm$^2$. Besides other properties, this ablation threshold strongly depends on the reflectivity of the coating material.[18] This motivates the use of an interface layer as discussed in Sec. II.
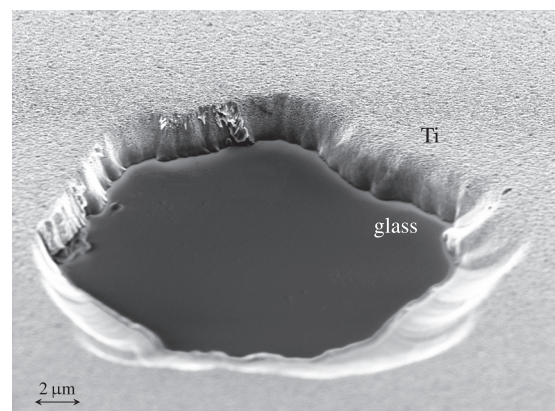
Besides a high laser damage threshold, a coherent coating with high adhesion on the glass surface is essential for LBO applications.

Hence, the homogeneity of the films is inspected after laser ablation using scanning electron microscopy (SEM). In Fig. 2, a SEM micrograph of an ablated spot is shown that illustrates a coherent and adherent coating. Using white light interferometry, the lateral profile from the glass surface (dark area in Fig. 2) to the remaining coating (gray area in Fig. 2) can be measured to determine the coating thickness assuming a complete ablation. Exemplarily, the thickness of an envisaged 2 $\mu$m Ti coating is measured as 2 $\pm$ 0.04 $\mu$m taking into account 17 ablation spots that are distributed over the whole glass target, see one ablation spot in Fig. 2. Hence, the coating methods that are described in Sec. II produce a coherent coating with a sufficient lateral homogeneity within 2%.

To analyze the composition of the coatings, exemplary pure Fe films of 2 $\mu$m thickness are analyzed using x-ray photoelectron spectroscopy (XPS). The XPS spectra, see Fig. 3, are analyzed and charge corrected by shifting all peaks to the aliphatic C 1s spectral component set to a binding energy of 285 eV. To remove contaminants from the sample surface, it is sputtered *in situ* with Ar$^+$ ions for 2 min. The XPS measurements are carried out before and after cleaning. The elements O, C, and Fe are detected in the overview spectra, see Fig. 3. Since the information depth of XPS is typically 5 nm–10 nm, only the outermost surface layer of the film is analyzed. Moreover, hydrogen, which is assumed to be also on the coating surface, cannot be detected by XPS. Before sputtering, the surface contains considerable amounts of C and O as well as N with an intensity close to the detection limit. These are surface contaminants and oxides acquired from the exposure to ambient air. The surface layers render the portion of Fe to only about 10%. After the sputtering process, the C peak decreases significantly, demonstrating the effective removal of the surface layer and the access of the analysis to the actual coating material. Traces of Ar with an intensity close to the detection limit are also detectable since it is contained in the gas mixture of the process, and part of the Ar ions impinging on the surface are incorporated in the growing film. After cleaning, the Fe 2p peak can be evaluated. According to the literature,[30] the Fe 2p$_{3/2}$ component can be exploited to estimate the proportion of metallic Fe after performing a peak fitting procedure. Hence, the proportion of metallic Fe could be estimated to be about 85% $\pm$ 1%, whereas the



**FIG. 1**. SEM micrograph of the ablation spot with a crater on the glass surface (a) and a zoom that visualizes the Fe/Ti coating in detail (b). The coating was blown-off with a laser energy density above the laser damage threshold at about 14 J/cm$^2$, creating a crater in the glass target. At the edge of the ablated spot where the laser energy is lower, a fraction of the melted material stays on the glass surface albeit the coating is almost ablated (b).



**FIG. 2**. SEM micrograph of an ablated spot on a glass target that is coherently coated with Ti with a measured thickness of 2.0 $\pm$ 0.04 $\mu$m.
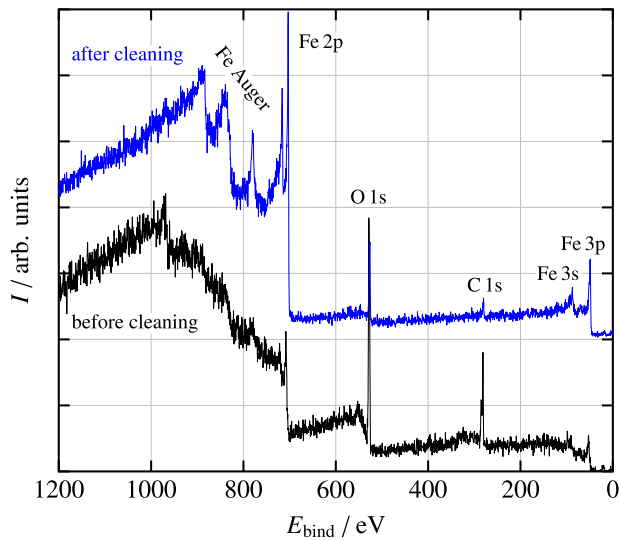
FIG. 3. XPS overview spectra with the intensity over the binding energy before (bottom) and after (top) cleaning the surface via sputtering.

proportion of Fe oxides is about 15% ± 1% showing a relatively pure coating with contaminants below 5%.

## IV. CHARACTERIZATION OF LBO INJECTION FOR IMPURITY TRANSPORT STUDIES IN WENDELSTEIN 7-X

As mentioned before, the coated glass targets are used to inject impurities into the plasma of W7-X by means of LBO. The characterization of the impurity injection itself is important for further analysis, e.g., the implementation of transport codes that can describe the particle transport due to diffusion and convection.

For the analysis of the composition of the injected material, spectra taken by the high-efficiency extreme ultraviolet (XUV/VUV) overview spectrometer (HEXOS)[31] are used. Despite the surface contamination with C, O, and N measured by XPS, see Sec. III, none of these impurities are found in the VUV spectra taken after an injection. Very weak Ti lines from the interface layer are possibly observed, but most of them are heavily superimposed by much stronger Fe lines and thus difficult to identify in the spectra due to the low concentration of about 2%. Hence, the contamination of the injected material is negligible and not taken into account for any further analysis based on LBO injection.

For modeling the impurity behavior in W7-X, it is important to know the amount and velocity of particles being injected into the plasma as atoms, clusters, and macro-particles. An optimal condition can be achieved for LBO impurity injection at high atom to cluster/macro-particle ratios. This requires a high laser energy volume density,[2,15,32,33] e.g., a high laser energy aimed at a thin coating. Additionally, the amount of clusters depends on the material.[15] The ablated amount of particles can be estimated after the ablation process taking into account the measurement of the coating thickness, as described in Sec. III, and the area of the ablated spot. Due to the

sufficient lateral homogeneity that is shown in Sec. III, the ablated volume and thus the amount of particles are inferred considering material specific quantities such as the molar volume. In addition, one needs to consider the fraction of ionized particles generated by the ablation process since ions are deflected by the strong magnetic fields in W7-X and cannot reach the plasma. Hence, it is assumed that only 20%–50% of the particles reach the LCFS.[34] This translates to about $10^{17}$ injected particles for a spot size of 4 $mm^2$.

Inside the plasma, the injected particles can be monitored in the visible spectral range with a video diagnostic system.[35] The event detection intelligent camera (EDICAM)[36] has the ability to simultaneously record visible radiation in independent regions of interest with different time resolution. When the injected particles reach the plasma, the neutrals as well as the lowest ionization stages start to emit in the deposition zone where the excitation becomes relevant. Thus, the location of the deposition zone as well as the dynamic behavior of the injected particles can be determined by measuring the emission in the visible spectral range, which, in the case of Fe, is mainly emitted from Fe(I) and Fe(II). This is exemplarily visualized in Fig. 4 that shows a time-integrated cross section picture taken inside the plasma vessel during a discharge and an injection of Fe by means of LBO. Additionally, the cross section of the field lines for the standard magnetic field configuration in the vacuum mapped in the poloidal plane of the LBO injection is shown. The injected Fe particles are visible as emission patterns (red for atoms, white for clusters and macro-particles), see also the inset in Fig. 4, in the deposition zone that is radially located at the LCFS. The temporal and spatial
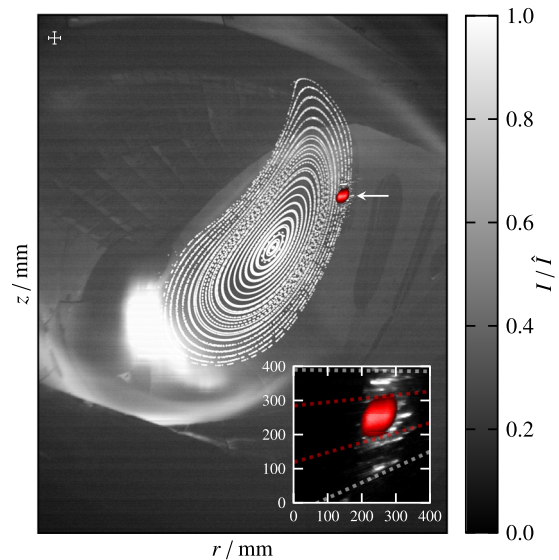


FIG. 4. Cross section picture of the normalized emission intensity *I* measured in the visible spectral range inside the plasma vessel during the LBO injection (Fe) together with field lines for the standard magnetic field configuration in vacuum for the experimental program 20171012.022. The emission pattern from the injected particles is highlighted in red for the atoms and white for clusters and macro-particles. The inset shows a magnification of the emission pattern together with dotted lines indicating the opening angle. The cross in the upper left corner represents the positioning accuracy of the field lines.

resolution ($\Delta z = \Delta r = 3$ mm, $\Delta t = 0.1$ ms) of the EDICAM is high enough to observe most of the clusters and macro-particles, individually. Hence, they can be easily distinguished from the fast and small atoms.

Since the poloidal plane of the LBO injection is almost perpendicular to the observation axis of the EDICAM, the angle as well as the velocity distribution of the injected particles can be estimated from the temporal evolution of the emission patterns shown in the inset of Fig. 4. An opening angle for atoms of about 15° is observed (red dotted line in the inset of Fig. 4), considering the spatial width of the radiating cloud and the distance between the LCFS, where the injected particles start to emit, and the surface of the glass target. The analysis of the angle distribution of clusters yields 30° (white dotted line in the inset of Fig. 4), possibly explained by the formation region in the edge of the ablation spot where the laser energy density is smaller compared to that at the center due to the laser beam profile. These angle distributions of the atoms and clusters are similar to those in the literature[2,15] and narrow enough to be a localized source of impurities in the W7-X plasma.

Thanks to the high time resolution of the EDICAM, the propagation speed of the radiating cloud of atoms, clusters, and macro-particles can be analyzed. The velocity of the injected particles is mainly the result of the momentum transfer during the ablation process (mostly in the horizontal direction) and is deflected by the gravitational force and drifts due to electric–magnetic fields. The normalized emission intensity distribution of the particles (see the inset of Fig. 4), vertically (a) and horizontally (b) integrated, is shown in Fig. 5 for a time duration of 17.5 ms. The clearly visible peak at $t - t_{LBO} = 0$ can be attributed to the atoms that are faster due to the lower mass compared to clusters and macro-particles. Assuming that the emitting atoms move radially from one side of the observed emission pattern to the other side (from $r_1 = 300$ mm to $r_2 = 200$ mm) within 0.1 ms yields in zero order to an averaged velocity of about 1 km/s as a lower limit. This is comparable with that reported in the literature[16,32,37,38] for the used laser energy density in the range of 2 J/cm$^2$–30 J/cm$^2$. After the bright pattern of atoms, a lower intensity can be assigned to slower clusters that can be tracked individually. The velocity of the clusters can be determined from the slope of the dotted lines (distance over time) in Fig. 5 representing the path of the emitting particles. The assumption of a constant velocity is well reflected by the measurement of the emission, especially for the radial movement. As a result, the horizontal velocity of the fastest quantifiable cluster is about $v_{r_1} = 0.1$ km/s, whereas the velocity of the slower clusters is about $v_{r_1} = 0.05$ km/s. The downward velocity is about $v_{z_1} = 0.05$ km/s and is one order of magnitude higher compared to the upward velocity $v_{z_2}$, indicating the impact of additional forces. Hence, the kinetic energy of injected particles ranges between 0.05 eV and 30 eV for the here shown Fe injection.

The temporal behavior of the radially integrated emission intensity, see Fig. 5(c), defines the source function and indicates that the particle cloud mainly consists of atoms since the intensity of the atomic beam is at least one order of magnitude higher compared to that of the clusters. In addition, the emission from the ablated material reaching the plasma is measured by a high photon throughput Czerny–Turner-like spectrometer, which uses aspherical quartz lenses for reduced transmission losses instead of mirrors. The emission at a central wavelength of 650 nm is focused onto a
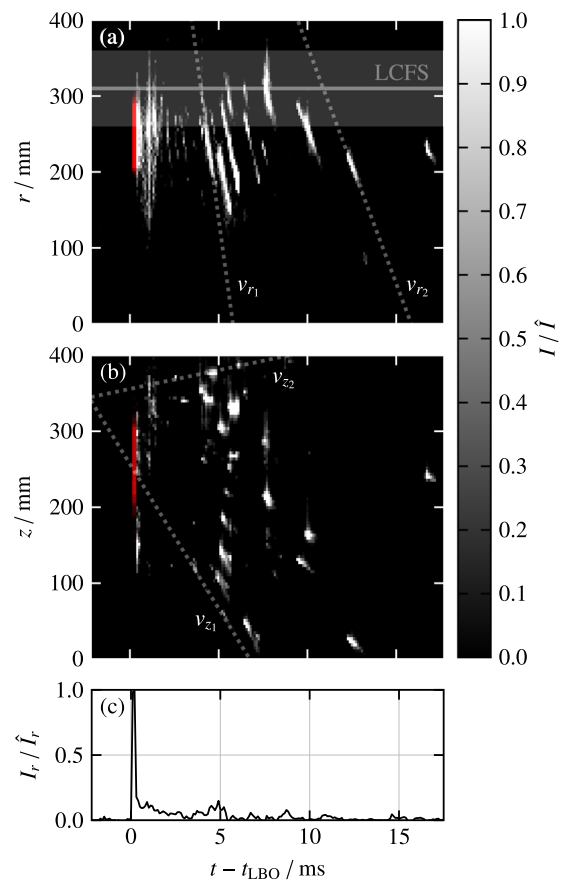


**FIG. 5**. Normalized emission intensity $I$ mainly of Fe(I) and Fe(II) (atoms in red, clusters and macro-particles in white) integrated over the vertical (a) and horizontal (b) axes over the time and the time trace (c) of the radially integrated normalized emission intensity (a) for the experimental program 20171012.022. The dotted lines indicate the path of the injected clusters and macro-particles. The slope of these lines describes the individual velocity $v$ of the particles. The radial position of the LCFS is indicated as a solid line in (a) together with a shaded area indicating the positioning accuracy.

camera with an electron multiplying charge-coupled device (EM-CCD) chip, which is operated in a burst mode setting that allows an exposure time of 35 $\mu$s. The first burst is triggered by a pulse received directly from the laser system, such that the start of the burst is synchronized with the firing of the laser. Exemplarily, after 0.25 ms, a sudden and sharp increase in the intensity is observed over the full spectrum, indicating that the atoms reach the plasma and start to emit. Besides a very intense Fe(I) line at 649.498 nm that is slightly overlapped with a weak O(V) line at 650.024 nm, several other lines associated with Fe(I) and Fe(II) appear in the spectra. In Fig. 6, the temporal behavior of the Fe(I) lines (mainly from 649.498 nm) is shown over the time (bottom axis) after the laser pulse, which was aimed on an Fe/Ti (thickness of 5 $\mu$m/0.1 $\mu$m) target. The velocity of the ablated atoms, see the top axis in Fig. 6, reaching the plasma can be derived from the time difference between the received trigger and the first emission observation. For this
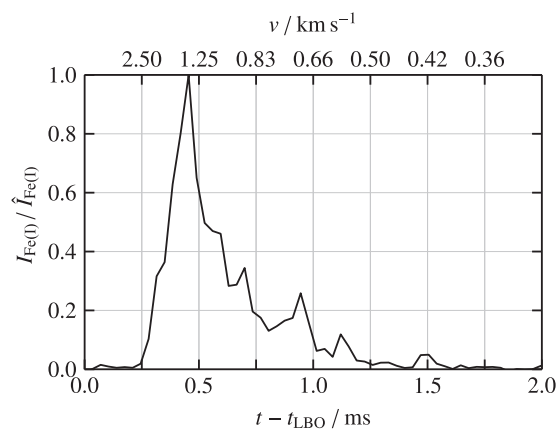
**FIG. 6**. Normalized emission intensity of Fe(I) over the time after the laser pulse (bottom axis) and the velocity (top axis) of injected atoms for the experimental program 20180906.038. The velocity can be estimated within the uncertainty of $\pm 5\%$ due to the inaccuracy of the distance between the glass target surface and the deposition zone at the LCFS.

simple estimation, it is assumed that the particles move linearly in time from the glass surface to the LCFS within a certain penetration depth without any retardation. Hence, uncertainties due to the distance estimation in the range of $\pm 5\%$ originate for the velocity determination of atoms for this specific ablation process. However, the velocity of the injected atoms is well in agreement with that reported in the literature[16,32,37,38] and the above-mentioned rough estimation.

## V. SUMMARY

Glass targets coated with Fe and Ti are exemplarily investigated with respect to their applicability for the impurity injection in W7-X. As a result, the glass targets and coatings have successfully been optimized for LBO studies, leading to an overall success of the system. The coating of the fused silica glass targets by means of PVD methods produces thin films with a lateral homogeneity within 2% and high purity with contaminants less than 5%. Additionally, these coated glass targets are qualified for this high laser energy LBO processing due to their high laser damage threshold. From a coating with a thickness of 5 $\mu$m, about $10^{17}$ particles can be injected close to the LCFS of W7-X with a velocity between 0.05 km/s and 1 km/s. The distribution of injected particles, in both space and velocity, is perfectly suitable for impurity transport studies and can be used as experimental input data for transport analysis codes.

## ACKNOWLEDGMENTS

## DATA AVAILABILITY

The data that support the findings of this study are available from the corresponding author upon reasonable request.

## REFERENCES

[1] M. Domke, S. Rapp, M. Schmidt, and H. P. Huber, Appl. Phys. A **109**, 409 (2012).
[2] E. S. Marmar, J. L. Cecchi, and S. A. Cohen, Rev. Sci. Instrum. **46**, 1149 (1975).
[3] S. A. Cohen, J. L. Cecchi, and E. S. Marmar, Phys. Rev. Lett. **35**, 1507 (1975).
[4] R. C. Isler, Nucl. Fusion **24**, 1599 (1984).
[5] R. Burhenn, Y. Feng, K. Ida, H. Maassberg, K. J. McCarthy, D. Kalinina, M. Kobayashi, S. Morita, Y. Nakamura, H. Nozato, S. Okamura, S. Sudo, C. Suzuki, N. Tamura, A. Weller, M. Yoshinuma, and B. Zurro, Nucl. Fusion **49**, 065005 (2009).
[6] B. Zurro, E. Hollmann, A. Baciero, M. A. Ochando, F. Medina, K. J. McCarthy, E. Blanco, E. de la Cal, D. Carralero, M. A. Pedrosa, and TJ-II Team, Nucl. Fusion **51**, 063015 (2011).
[7] Th. Wegner, B. Geiger, F. Kunkel, R. Burhenn, T. Schröder, C. Biedermann, B. Buttenschön, G. Cseh, P. Drews, O. Grulke, K. Hollfeld, C. Killer, G. Kocsis, T. Krings, A. Langenberg, O. Marchuk, U. Neuner, D. Nicolai, G. Offermanns, N. A. Pablant, K. Rahbarnia, G. Satheeswaran, J. Schilling, B. Schweer, T. Szepesi, H. Thomsen, and W7-X Team, Rev. Sci. Instrum. **89**, 073505 (2018).
[8] M. W. Kissick, E. D. Fredrickson, J. D. Callen, C. E. Bush, Z. Chang, P. C. Efthimion, R. A. Hulse, D. K. Mansfield, H. K. Park, J. F. Schivell, S. D. Scott, E. J. Synakowski, G. Taylor, and M. C. Zarnstorff, Nucl. Fusion **34**, 349 (1994).
[9] F. Ryter, R. Neu, R. Dux, H.-U. Fahrbach, F. Leuterer, G. Pereverzev, J. Schweinzer, J. Stober, W. Suttrop, ASDEX Upgrade Team, F. D. Luca, A. Jacchia, and J. E. Kinsey, Nucl. Fusion **40**, 1917 (2000).
[10] K. McCormick, Rev. Sci. Instrum. **56**, 1063 (1985).
[11] J. S. Bakos, G. Burger, I. B. Földes, P. E. Giese, P. N. Ignácz, G. Petravich, J. Szigeti, and S. Zoletnik, Plasma Phys. Controlled Fusion **31**, 693 (1989).
[12] D. Michaud, G. G. Ross, E. Haddad, H. H. Mai, A. Pospieszczyk, and J. P. St-Germain, Rev. Sci. Instrum. **63**, 5698 (1992).
[13] S. Sasaki, S. Takamura, Y. Uesugi, Y. Ohkouchi, and K. Kadota, Rev. Sci. Instrum. **64**, 2277 (1993).
[14] J. F. Friichtenicht, Rev. Sci. Instrum. **45**, 51 (1974).
[15] D. Manos, D. Ruzic, R. Moore, and S. Cohen, J. Vac. Sci. Technol. **20**, 1230 (1982).
[16] S. K. Mattoo, L. Wirtz, A. Pospieszczyk, and B. Schweer, Nucl. Instrum. Methods Phys. Res., Sect. B **124**, 579 (1997).
[17] G. Heise, M. Englmaier, C. Hellwig, T. Kuznicki, S. Sarrach, and H. P. Huber, Appl. Phys. A **102**, 173 (2011).
[18] M. Domke, L. Nobile, S. Rapp, S. Eiselen, J. Sotrop, H. P. Huber, and M. Schmidt, Phys. Procedia **56**, 1007 (2014).
[19] F. H. Karg, Sol. Energy Mater. Sol. Cells **66**, 645 (2001).
[20] S. Zoppel, H. Huber, and G. A. Reider, Appl. Phys. A **89**, 161 (2007).
[21] J. Bohandy, B. F. Kim, and F. J. Adrian, J. Appl. Phys. **60**, 1538 (1986).
[22] T. Klinger, T. Andreeva, S. Bozhenkov, C. Brandt, R. Burhenn, B. Buttenschön, G. Fuchert, B. Geiger, O. Grulke, H. Laqua, N. Pablant, K. Rahbarnia, T. Stange, A. von Stechow, N. Tamura, H. Thomsen, Y. Turkin, Th. Wegner, and W7-X Team, Nucl. Fusion **59**, 112004 (2019).
[23] A. Langenberg, N. A. Pablant, Th. Wegner, P. Traverso, O. Marchuk, T. Bräuer, B. Geiger, G. Fuchert, S. Bozhenkov, E. Pasch, O. Grulke, F. Kunkel, C. Killer, D. Nicolai, G. Satheeswaran, K. P. Hollfeld, B. Schweer, T. Krings, P. Drews, G. Offermanns, A. Pavone, J. Svensson, J. A. Alonso, R. Burhenn, R. C. Wolf, and W7-X Team, Rev. Sci. Instrum. **89**, 10G101 (2018).
[24] A. Langenberg, F. Warmer, G. Fuchert, O. Marchuk, A. Dinklage, Th. Wegner, J. A. Alonso, S. Bozhenkov, K. J. Brunner, R. Burhenn, B. Buttenschön, P. Drews, B. Geiger, O. Grulke, M. Hirsch, U. Höfel, K. P. Hollfeld, C. Killer, J. Knauer,

T. Krings, F. Kunkel, U. Neuner, G. Offermanns, N. A. Pablant, E. Pasch, K. Rahbarnia, G. Satheeswaran, J. Schilling, B. Schweer, H. Thomsen, P. Traverso, R. C. Wolf, and W7-X Team, Plasma Phys. Controlled Fusion **61**, 014030 (2018).

[25]B. Geiger, Th. Wegner, C. D. Beidler, R. Burhenn, B. Buttenschön, R. Dux, A. Langenberg, N. A. Pablant, T. Pütterich, Y. Turkin, T. Windisch, V. R. Winters, M. Beurskens, C. Biedermann, K. J. Brunner, G. Cseh, H. Damm, F. Effenberg, G. Fuchert, O. Grulke, J. H. Harris, C. Killer, J. Knauer, G. Kocsis, A. Krämer-Flecken, T. Kremeyer, M. Krychowiak, O. Marchuk, D. Nicolai, K. Rahbarnia, G. Satheeswaran, J. Schilling, O. Schmitz, T. Schröder, T. Szepesi, H. Thomsen, H. Trimiño Mora, P. Traverso, D. Zhang, and W7-X Team, Nucl. Fusion **59**, 046009 (2019).

[26]K. Ida, R. J. Fonck, S. Sesnic, R. A. Hulse, and B. LeBlanc, Phys. Rev. Lett. **58**, 116 (1987).

[27]A. Dinklage, K. J. McCarthy, C. Suzuki, N. Tamura, Th. Wegner, H. Yamada, J. Baldzuhn, K. J. Brunner, B. Buttenschön, H. Damm, P. Drewelow, G. Fuchert, M. Hirsch, U. Hoefel, H. Kasahara, J. Knauer, D. Maier, J. Miyazawa, G. Motojima, T. Oishi, K. Rahbarnia, T. Sunn Pedersen, R. Sakamoto, R. C. Wolf, D. Zhang, and W7-X Team, Nucl. Fusion **59**, 076010 (2019).

[28]A. Langenberg, Th. Wegner, N. A. Pablant, O. Marchuk, B. Geiger, N. Tamura, R. Bussiahn, M. Kubkowska, A. Mollén, P. Traverso, H. M. Smith, G. Fuchert, S. Bozhenkov, H. Damm, E. Pasch, K.-J. Brunner, J. Knauer, M. Beurskens, R. Burhenn, R. C. Wolf, and W7-X Team, Phys. Plas. **27**, 052510 (2020).

[29]J. H. Powell, C. F. Oxley, and J. M. Blocher, Jr., *Vapor Deposition* (Wiley, 1967).

[30]A. P. Grosvenor, B. A. Kobe, M. C. Biesinger, and N. S. McIntyre, Surf. Interface Anal. **36**, 1564 (2004).

[31]W. Biel, G. Bertschinger, R. Burhenn, R. König, and E. Jourdain, Rev. Sci. Instrum. **75**, 3268 (2004).

[32]J. S. Bakos, I. B. Földes, P. N. Ignácz, G. Kocsis, J. Szigeti, and J. Kovács, Opt. Commun. **74**, 374 (1990).

[33]J. S. Bakos, I. B. Földes, P. N. Ignácz, and G. Kocsis, J. Appl. Phys. **69**, 1231 (1991).

[34]K. Assmussen, "Untersuchungen zum verhalten von wolfram in tokamak-plasmen," IPP Report 10/2, Max-Planck-Institut für Plasmaphysik, Garching, 1996.

[35]G. Kocsis, T. Baross, C. Biedermann, G. Bodnár, G. Cseh, T. Ilkei, R. König, M. Otte, T. Szabolics, T. Szepesi, and S. Zoletnik, Fusion Eng. Des. **96-97**, 808 (2015).

[36]S. Zoletnik, T. Szabolics, G. Kocsis, T. Szepesi, and D. Dunai, Fusion Eng. Des. **88**, 1405 (2013).

[37]T. Yamauchi, M. Nagami, and S. Sengoku, Jpn. J. Appl. Phys., Part 1 **19**, 1737 (1980).

[38]J. Szigeti, J. S. Bakos, G. Bürger, P. N. Ignácz, M. Á. Kedves, and L. Matus, Plasma Sources Sci. Technol. **5**, 32 (1996).